Microstructure evolution and mechanical properties of the Mg-7Zn-xY-0.6Zr ($x = 6$, 9, 12 wt.%) alloys

Z. Q. Zhang*, S. Q. Yin, X. Liu, L. Bao, W. Y. Hu, Q. C. Le, J. Z. Cui

*Key Lab of Electromagnetic Processing of Materials, Ministry of Education, Northeastern University,
Shenyang 110819, P. R. China*

Abstract

Mg-7Zn-xY-0.6Zr ($x = 6$, 9, 12 wt.%) alloys have been designed to investigate the effects of Y content on the microstructure and mechanical properties. The results show that Y content plays a key role in the phase composition and mechanical properties of the investigated Mg-7Zn-xY-0.6Zr alloys. With the Y content increasing from 6 to 12 %, the phase composition transformed from α-Mg + W-phase ($Mg_3Y_2Zn_3$) to α-Mg + X-phase ($Mg_{12}YZn$). The amount of X-phase increases rapidly, and W-phase decreases accordingly. Furthermore, the W-phase distributes alternatively with the X-phase, due to the specific local Y/Zn mole ratio at the final solidifying stage. After extrusion, the phase composition and corresponding volume fraction have great influence on mechanical properties. The X-phase is in favour of high strength and the W-phase makes for good plasticity. The as-extruded Mg-7Zn-12Y-0.6Zr alloy establishes the highest strength with an ultimate tensile and yield tensile strength of 416 MPa and 302 MPa, respectively.

K e y   w o r d s: Mg-Zn-Y-Zr, extrusion, casting and solidification, microstructures, mechanical properties

1. Introduction

Magnesium alloys have great potential for applications in automotive, aerospace, and 3C industries, due to low density, dimension stability, non-pollution, high specific strength, and specific stiffness [1]. What is more, it has been reported that magnesium alloys also have excellent anti-vibration, thermal conductivity, electromagnetic shielding characteristic, etc. [2, 3]. Currently, many investigations have been done on Mg-Al, Mg-RE (RE is rare earth) and Mg-Zn alloys. $Mg_{17}Al_{12}$ phase should be the common strengthening phase in the Mg-Al alloys, which, however, are still limited at elevated temperatures [1]. RE elements have often been added into magnesium alloys to improve the mechanical properties, especially at elevated temperatures [4]. However, Mg-RE alloys have been limited to some components due to their expensive cost. Mg-Zn alloys have strong precipitation strengthening effects, due to the dispersive MgZn and $MgZn_2$ phases [5, 6], but the MgZn and $MgZn_2$ phases perform badly

as the $Mg_{17}Al_{12}$ phase at elevated temperatures.

Even so, many scholars believe that the ternary Mg-Zn-Y system is efficient enough to improve the mechanical properties [7], which have been the most widely researched and developed. The element Y has strong solution strengthening and ageing strengthening effects because of its large equilibrium solid solubility in Mg matrix (12.5 wt.% [8]). Meanwhile, the ternary equilibrium phases: W-phase ($Mg_3Zn_3Y_2$, cubic structure) [9], I-phase (Mg_3Zn_6Y, icosahedral quasicrystal structure) [10], and X-phase ($Mg_{12}ZnY$, long period stacking ordered structure) [9] have shown outstanding effects on the microstructures and mechanical properties of the Mg-Zn-Y alloys [11–17].

However, most of these studies have focused on the Mg-Zn-Y-Zr alloys with either low Zn content or trace Y content [18]. There are still few reports on the microstructure and mechanical properties of Mg-Zn-Y alloys with both high Zn and Y content. Although phase composition could be obtained from thermodynamic calculation or phase diagrams, the detail phase

---

*Corresponding author: tel.: +86 24 83689825; e-mail address: zqzhang@mail.neu.edu.cn

T a b l e 1. Actual chemical composition of the investigated alloys (wt.%)

Nominal composition	Actual chemical composition (wt.%)			
	Zn	Y	Zr	Mg
Mg-7Zn-6Y-0.6Zr	6.89	5.73	0.48	Bal.
Mg-7Zn-9Y-0.6Zr	6.99	8.91	0.46	Bal.
Mg-7Zn-12Y-0.6Zr	7.04	11.8	0.43	Bal.

Fig. 1. XRD patterns of as-cast Mg-Zn-Y-Zr alloys.

quantity and distribution were still rarely reported when the Zn and Y addition are both over 6 wt.%. Meanwhile, the corresponding effects on the mechanical properties of the high alloying ternary Mg-Zn-Y alloys are also missing. In the present study, three Mg-7Zn-xY-Zr ($x = 6$, 9, 12 wt.%) alloys have been prepared to investigate the microstructure and mechanical properties of the Mg-Zn-Y-Zr alloys with both high Zn and Y content.

2. Materials and methods

Mg-7Zn-xY-0.6Zr alloys ($x = 6$, 9, and 12 %) were prepared with pure Mg (99.8 wt.%), pure Zn (99.9 wt.%), Mg-30 wt.% Zr master alloys and Mg-50 wt.% Y master alloys by direct electrical resistance melting in a mild steel crucible at 710 ℃ and casting into a pre-heated steel mould (~ 200 ℃) under cover of mixed SF_6 and CO_2. The chemical compositions of the investigated alloys were determined by an inductively coupled plasma mass spectrometry. The casting ingots were 60 mm in diameter and 150 mm in height. Table 1 shows the actual chemical composition of the investigated alloys. After casting process, the ingots were homogenized at 510 ℃ for 16 h. Then the ingots were machined into ø 47 mm cylinders with a length of 100 mm and were indirectly extruded into ø 12 mm rods with a speed of 5.6 cm s^{-1} in a ø 50 mm extruding container at 400 ℃. Meanwhile, the extrusion ratio was 15 : 1, and the container and mould were preheated to 350 ℃. The rods were machined into tensile specimens of 6 mm gauge diameter and 25 mm gauge length according to the ASTM standard B557M-10. The tensile direction was parallel to the extrusion direction. The tensile test was performed at room temperature by using a Shimadzu AG-X (100 kN) machine (the speed of tensile test was 1 mm min^{-1}).

The microstructure of the alloys was observed by an optical microscope (OM) and scanning electron microscope (SEM) coupled with an energy dispersive X-ray analyser (EDS). The phase analyses were performed with an X-ray diffractometer (XRD). The volume fraction of the second phase was estimated by
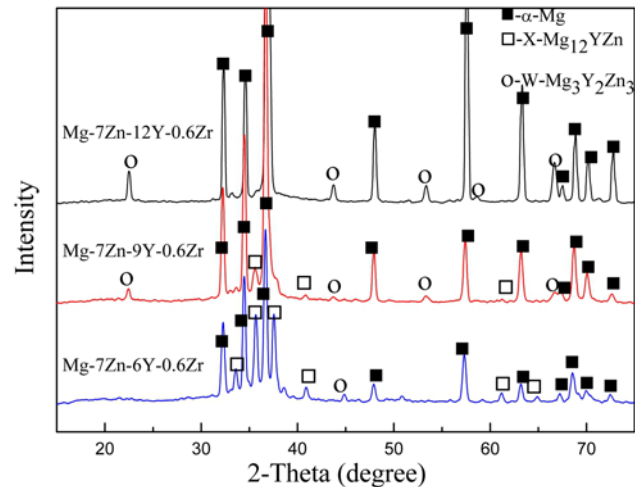
image analysis technique using at least ten areas for each alloy.

3. Results

3.1. The microstructure of as-cast Mg-Zn-Y-Zr alloys

Figure 1 shows the XRD patterns of the as-cast alloys. It could be seen that Mg-7Zn-6Y-0.6Zr alloy mainly consists of α-Mg solid solution and W-phase as shown in Fig. 1. With the Y content increasing to 9 wt.%, the as-cast alloy mainly consists of α-Mg solid solution, X-phase and W-phase. However, as the Y content further increases to 12 wt.%, the W-phase is almost replaced by the X-phase in the as-cast alloy. The phase transformation should be deeply attributed to the drastic Y/Zn mole ratio change of the investigated alloys [19].

Figure 2 shows the optical microstructure of the as-cast alloys. The as-cast Mg-7Zn-6Y-0.6Zr consists of α-Mg matrix and black discontinuous grain boundary reticular eutectic. According to the XRD pattern in Fig. 1, this reticular eutectic should be the cubic W-phase, whose volume fraction is about 19 %. With the increasing Y addition, the second phase transforms sharply from the eutectics into thick plates and alternate minor black phase (total volume fraction is ~ 55 %), as shown in Fig. 2b. The grey second phase is similar to the widely reported X-phase with an LPSO structure [20, 21], while the minor black phase should belong to the reducing W-phase. Furthermore, when Y content increased to 12 wt.%, the black eutectic phase almost disappeared, but the grey phase quantity grows slowly, as clearly shown in Fig. 2c. The volume fraction of the grey plate is about 65 % in the Mg-7Zn-
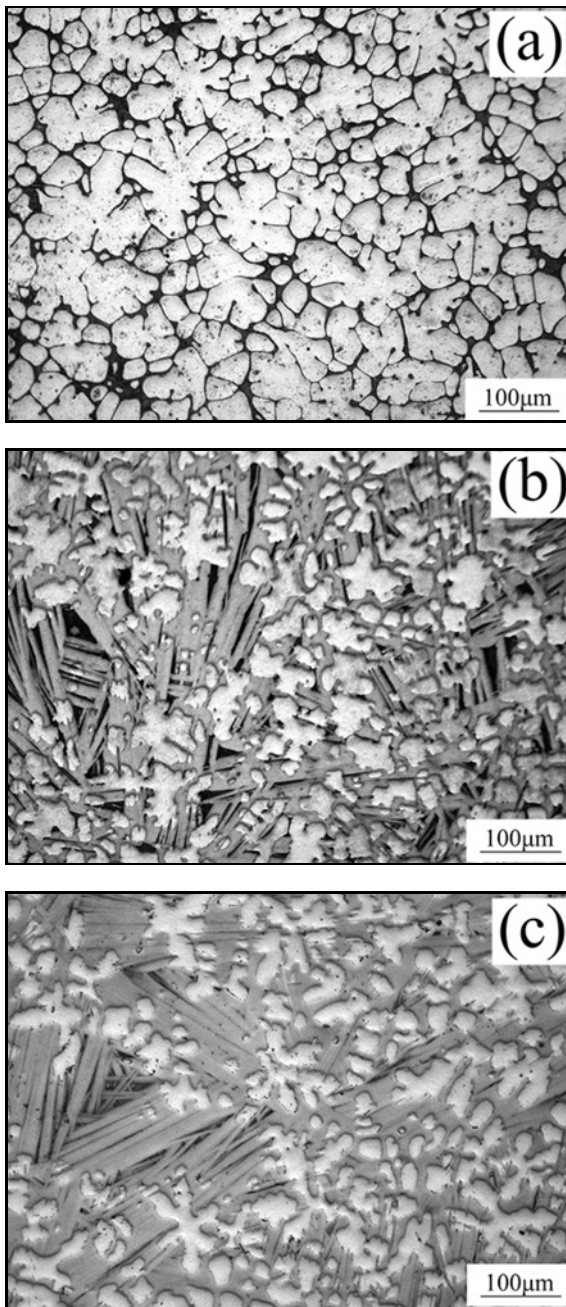
Fig. 2. Optical micrographs of as-cast Mg-Zn-Y-Zr alloys: (a) Mg-7Zn-6Y-0.6Zr, (b) Mg-7Zn-9Y-0.6Zr, (c) Mg-7Zn--12Y-0.6Zr.

Fig. 3. Backscattered electron images of as-cast Mg-Zn-Y--Zr alloys: (a) Mg-7Zn-6Y-0.6Zr, (b) Mg-7Zn-9Y-0.6Zr, (c) Mg-7Zn-12Y-0.6Zr.

Table 2. The corresponding EDX results in Fig. 3

Point	Mg (at.%)	Zn (at.%)	Y (at.%)
A	53.1	27.5	19.4
B	89.1	4.7	5.2
C	73.6	15.4	11.0

-12Y-0.6Zr alloy, almost covering the α-Mg matrix.

Figure 3 shows the backscattered electron images of as-cast Mg-Zn-Y-Zr alloys and Table 2 lists the corresponding EDX results in Fig. 3. The α-Mg matrix occupies the darkest contrast. Figure 3a shows that the reticular eutectics are concentrated along the grain boundaries in the Mg-7Zn-6Y-0.6Zr alloys. The EDX has been conducted to examine the composition of reticular eutectics (point A in Fig. 3a, Mg-19.4 at.% Y-27.5 at.% Zn). Th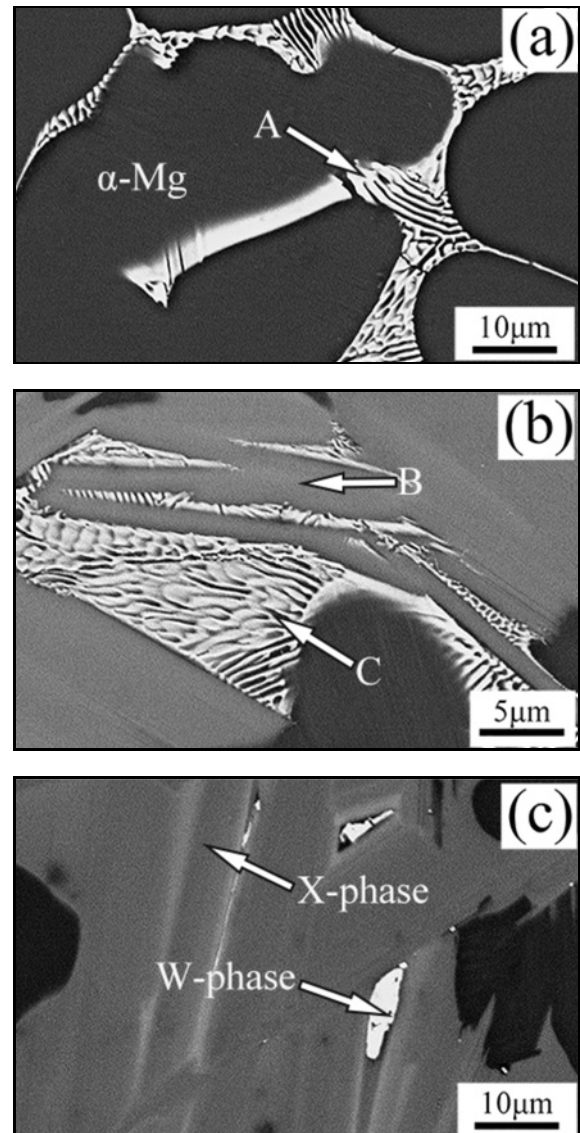e atomic ratio of Y and Zn is close to $2:3$, thus it is confirmed as the W-phase, which is in accordance with the XRD pattern in Fig. 1.

Figure 3b shows that the as-cast Mg-7Zn-9Y-0.6Zr alloy includes grey plates and similar white eutectics. The grey plate phases are composed of Mg, Y, and

Zn elements determined by EDX (point B in Fig. 3b), and the atomic ratio of Y and Zn is nearly 1 : 1. Thus, it should be the X-phase ($Mg_{12}YZn$). The eutectic (point C in Fig. 3b) is similar to that in the Mg--7Zn-6Y-0.6Zr alloy. Therefore, the as-cast Mg-7Zn--9Y-0.6Zr alloy should include α-Mg, X-phase and W-phase. The phase composition of Mg-7Zn-12Y-0.6Zr is close to that of the Mg-7Zn-9Y-0.6Zr alloy. However, the amount of W-phase eutectic decreases owing to a higher Y content. Thus, the investigated Mg-Zn-Y-Zr alloys with higher Y addition should consist of α-Mg, large amount of X-phase besides minor W-phase eutectic.

3.2. Microstructure of as-extruded Mg-Zn-Y-Zr alloys

Figure 4 shows the longitudinal sections of the as--extruded Mg-7Zn-xY-0.6Zr alloys along the extrusion direction. The dynamic recrystallization (DRX) occurs in all three alloys after indirect extrusion and the second phases are elongated along the extrusion direction. The average grain size of the as-extruded Mg-7Zn-6Y-0.6Zr is approximately 5 μm, and a quantity of fine particles distributes along the extrusion direction. The microstructures of the as-extruded Mg--7Zn-9Y-0.6Zr and Mg-7Zn-12Y-0.6Zr alloys are quite different from Mg-7Zn-6Y-0.6Zr alloy, as shown in Figs. 4b,c. There is a large amount of fibre-like second phase elongated along the extrusion direction. This fibre-like phase should be the elongated X-phase during the extrusion process. Furthermore, the amount of fibre-like second phase in Mg-7Zn-12Y-0.6Zr is quite close to the Mg-7Zn-9Y-0.6Zr. However, the grain size of both the Mg-7Zn-9Y-0.6Zr and Mg-7Zn-12Y-0.6Zr is hard to estimate due to the too many cracked and elongated X-phases almost covering the matrix.

Figure 5 shows the SEM images of the as-extruded alloys. It could be clearly seen that the eutectics were cracked into a lot of white particles with different size distributing along the extrusion direction in Mg-7Zn--6Y-0.6Zr. For the Mg-7Zn-9Y-0.6Zr alloy, it is further confirmed that a large quantity of white and elongated X-phase is distributing throughout the α-Mg matrix. What is more, a quantity of fine white particles distributes dispersedly around these elongated X-phase boundaries, as shown in Fig. 5b. A quantity of elongated X-phases also distributes similarly in the as-extruded Mg-7Zn-12Y-0.6Zr alloy, but the fine white particles are missing, as shown in Fig. 5c. Meanwhile, Fig. 5d shows some DRXed grains near the cracked second phase in the as-extruded Mg-7Zn--12Y-0.6Zr alloy, and these grains are just a few micrometres in diameter. Figure 6 shows the XRD patterns of the as-extruded alloys. It suggests that the no phase transformation occurred during the indirect hot extrusion.
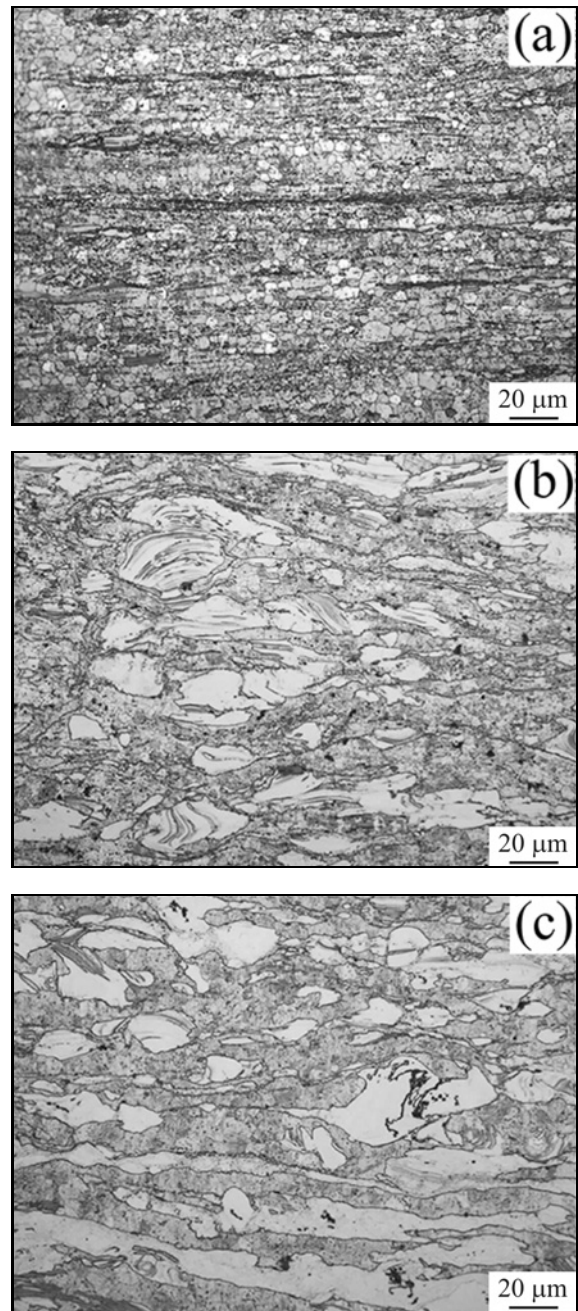

Fig. 4. Optical micrographs of as-extruded Mg-Zn-Y-Zr alloys: (a) Mg-7Zn-6Y-0.6Zr, (b) Mg-7Zn-9Y-0.6Zr, (c) Mg--7Zn-12Y-0.6Zr.

3.3. Mechanical properties of as-extruded Mg-Zn-Y-Zr alloys

Figure 7 shows the mechanical properties of as-extruded alloys at room temperature. The Y addition markedly influences the mechanical properties of the as-extruded alloys. The Mg-7Zn-6Y-0.6Zr with lowest Y content owns the lowest strength, but the maximum elongation. Its yield tensile strength (YTS), ultimate tensile strength (UTS), and elongation are 216,
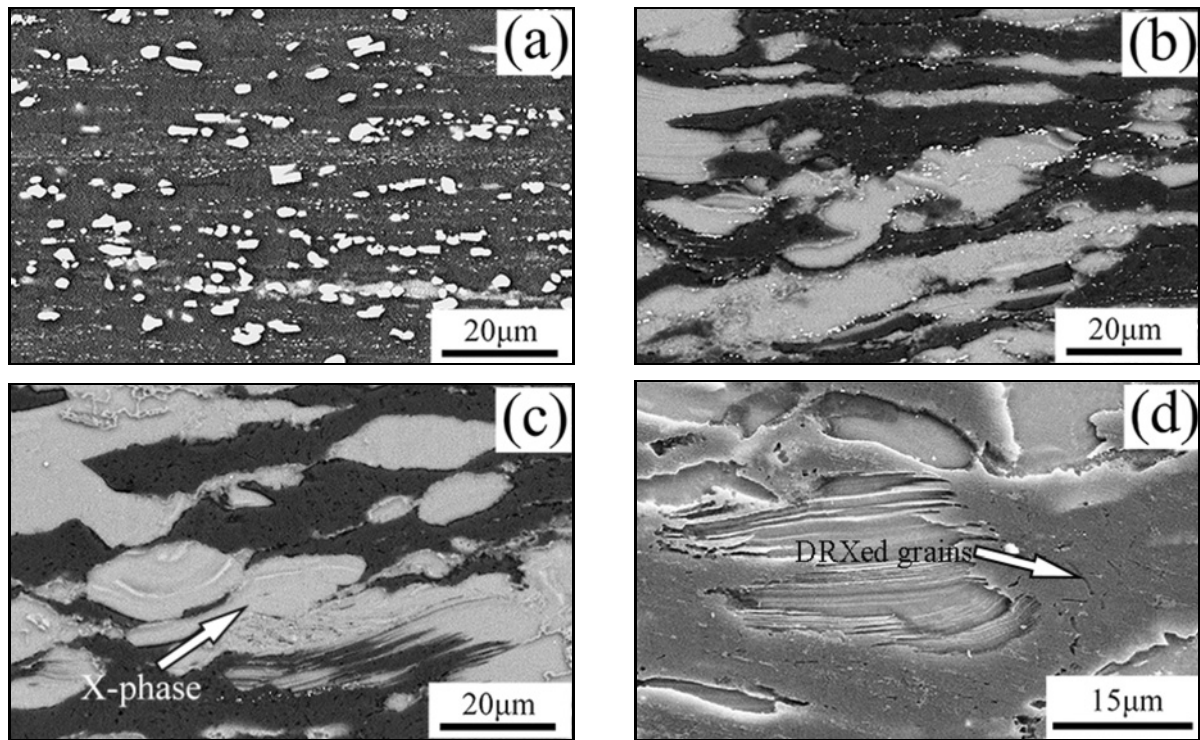
Fig. 5. SEM images of as-extruded Mg-Zn-Y-Zr alloys: (a) Mg-7Zn-6Y-0.6Zr, (b) Mg-7Zn-9Y-0.6Zr, (c), (d) Mg-7Zn-12Y--0.6Zr.
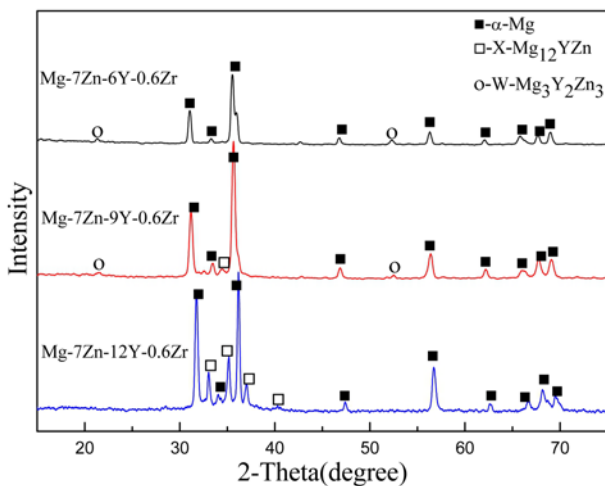

Fig. 6. XRD patterns of as-extruded Mg-Zn-Y-Zr alloys.

Fig. 7. Mechanical properties of as-extruded Mg-Zn-Y-Zr alloys.

287 MPa, and 13.7 %, respectively. When the Y content is increased to 9 wt.%, the YTS and UTS are improved greatly, but the elongation decreases drastically. It is noted that the YTS, UTS, and elongation are 274, 404 MPa, and 6.5 %, respectively. It shows that yield strength and tensile strength increased by 27 and 41 %, respectively. The strength is improved marginally when the Y addition is further up to 12 wt.%. Even so, the elongation becomes quite limited. The YTS and UTS of Mg-7Zn-12Y-0.6Zr increase to 302 MPa and 416 MPa separately.
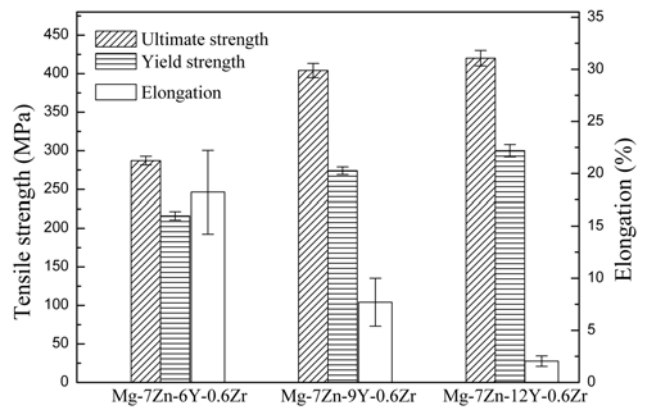
4. Discussion

In the present work, phase composition of the investigated as-cast alloys transformed from α-Mg + W-phase to α-Mg + X-phase as Y addition increased from 6 to 12 wt.%. It was also consistent with the previous thermodynamic calculation and Mg-Zn-Y ternary phase diagram [22]. Even so, the alternative distribution of W- and X-phase is an interesting phenomenon not concerned widely in the previous reports.

Generally, the conventional casting process should be considered as a non-equilibrium solidifying process,
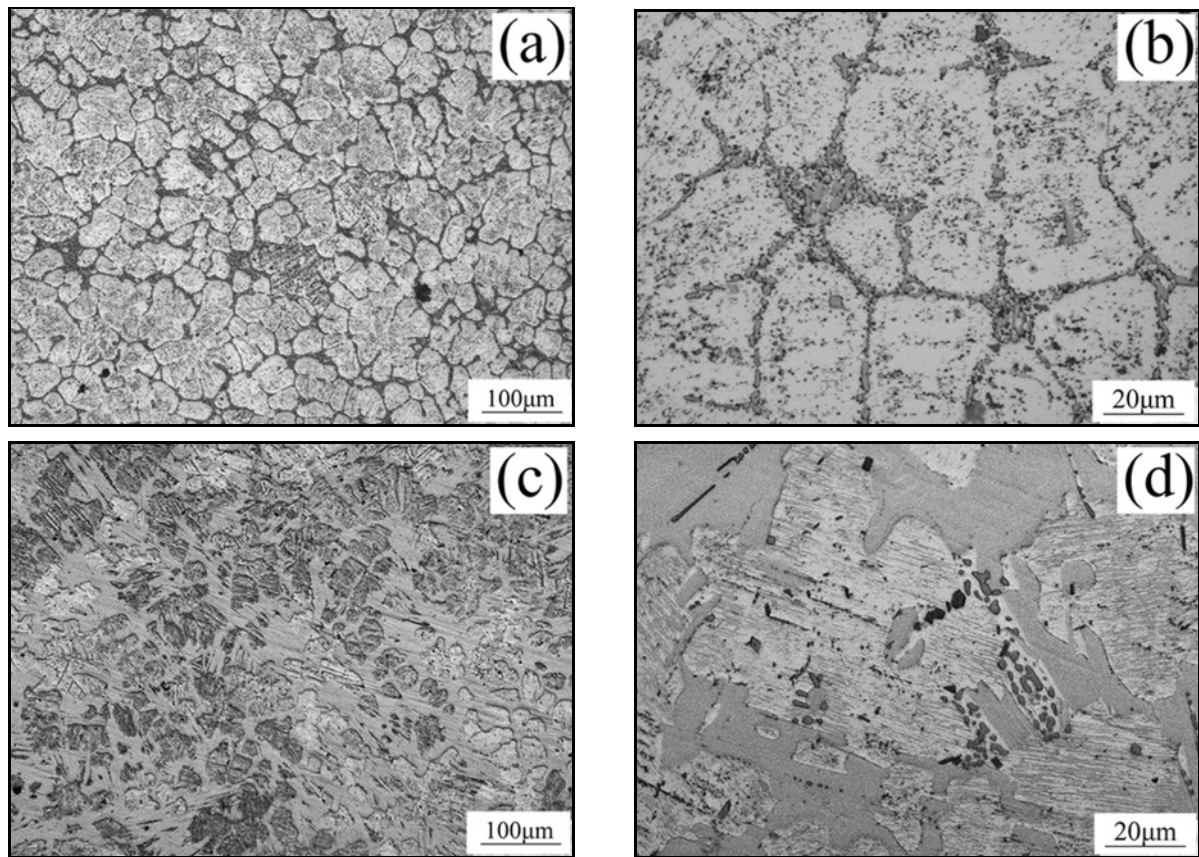
Fig. 8. Optical micrographs of the as-homogenized alloys: (a), (b) Mg-7Zn-6Y-0.6Zr; (c), (d) Mg-7Zn-9Y-0.6Zr.

due to the fast cooling rate. If one assumes no diffusion in the solid but perfect mixing in the liquid, the mean composition of the solidified α-Mg crystals is always lower than the nominal composition of the alloy, and the solute Y and Zn are pushed into the liquid next to the solid-liquid interface. With the nucleation and growth of primary α-Mg in progress, more and more solute Y and Zn are distributing in the liquid around the primary α-Mg crystal nucleus. For Mg-7Zn-6Y--0.6Zr, the Y/Zn concentration ratio of the liquid is very close to that of W-phase ($Mg_3Y_2Zn_3$), then the eutectics precipitated around the grain boundaries at the last solidifying stage, as shown in Fig. 3a. For Mg--7Zn-9Y-0.6Zr and Mg-7Zn-12Y-0.6Zr, the Y/Zn concentration ratio in the liquid is very close to that in X-phase ($Mg_{12}YZn$). Then, the X-phase could precipitate correspondingly. With the solidification further in progress and decreasing temperature, the reduced solute diffusion rate allows a concentration fluctuation for Y and Zn solute in the localized micro-areas. Then, Y/Zn mole ratio in some local areas might be close to that of W-phase ($Mg_3Y_2Zn_3$) [23]. On the other hand, there are no sufficient Mg atoms in the remnant liquid to participate in the precipitation of X-phase at these micro-areas. Hence, it is quite reasonable for the W-phase appearing next to the precipitated X-phase. With such solidifying sequence, it could not only ex-

plain the solidifying of X- and W-phase but also makes sense that the eutectic W-phase is solidifying alternately with the X-phase, as shown in Fig. 2c.

After extrusion, the matrix was dynamically recrystallized and the second phase cracked along the extrusion direction. A lot of white particles could be observed in the as-extruded Mg-7Zn-6Y-0.6Zr. Meanwhile, similar white but fine particles are also found around the broken X-phase in the as-extruded Mg--7Zn-9Y-0.6Zr alloy. This special distribution should be attributed to the homogenization process before extrusion. Figure 8 shows the microstructures of the as-homogenized Mg-7Zn-6Y-0.6Zr and Mg-7Zn-9Y--0.6Zr. It can be seen that eutectic W-phase disrupted into dispersed particles, distributing discontinuously throughout the matrix, as shown in Fig. 8b. It suggests that W-phase eutectic is not very thermostable during the homogenization treatment. Thus, it could be seen that these remnant particles migrated along the extrusion direction during the deformation process, as shown in Fig. 5a. From the Fig. 8c, it can be seen that the X-phase was barely dissolved into the α-Mg matrix, and some undissolved particles distributed along this stable X-phase, as shown in Fig. 8d. These particles should belong to undissolved W-phase. Therefore, it is reasonable to find the fine particles along the elongated X-phase, as shown in Fig. 5b. For

the as-extruded Mg-7Zn-12Y-0.6Zr, it is hard to find the similar particles, because it contains quite minor W-phase.

The results show that different Y content can influence the microstructure and mechanical properties of as-extruded Mg-Zn-Y-Zr alloys considerably through phase composition and volume fractions. It could be seen that dynamic recrystallization occurs in all three investigated alloys, as shown in Fig. 4. The grain size of the three alloys is very close to just a few micrometres. With the increasing Y addition, the discontinuous W-phase eutectic was sharply replaced by the thick and compact X-phase plate. Also, the volume fraction of the X-phase was much larger than that of W-phase. Consequently, the microstructures of the as--extruded alloys vary evidently, so do the mechanical properties.

From Figs. 4, 5, it can be seen that there is a quantity of the elongated X-phases along the hot extrusion direction in Mg-7Zn-9Y-0.6Zr alloy extruded bars. The interfaces between these phases and α-Mg matrix are consistent with the tensile direction. Therefore, shear deformation mainly occurs at these elongated X-phases when tensile loads are consistent with extrusion direction. That is, these elongated X-phases distributed along extrusion direction could be considered as beneficial fibres in the composite materials to strengthen the matrix [24]. However, this is not available for the Mg-7Zn-6Y-0.6Zr alloy, as shown in Fig. 5a. It is suggested that the second-phase strengthening performs outstandingly in toughening the alloys in the present work.

As can be seen from Figs. 4b,c, Mg-7Zn-12Y-0.6Zr contains similar quantity of X-phases to the Mg-7Zn--9Y-0.6Zr. Consequently, the UTS are quite close for these two extruded alloys. However, due to the large amount of fibre-like X-phase, the dislocation movement is deeply suppressed so that the elongation decreases sharply. The phases in Mg-7Zn-6Y-0.6Zr are less, finer and uniformly dispersed in the matrix. In this way, its elongation is much higher.

5. Conclusions

In this work, the phase composition of the investigated alloys is different due to the different Y contents. The phase composition transforms from α-Mg + W--phase ($Mg_3Y_2Zn_3$) to α-Mg + X-phase ($Mg_{12}YZn$) as Y addition increased from 6 to 12 wt.%. The amount of X-phase increased rapidly, and W-phase decreased accordingly. Furthermore, the W-phase distributed alternatively with the X-phase, due to the specific Y/Zn mole ratio in local areas. After extrusion, the Y content has a great influence on mechanical properties via controlling the phase composition and corresponding volume fraction. The X-phase is in favour of high strength but poor plasticity, and it is opposite for the W-phase. The as-extruded Mg-7Zn-12Y-0.6Zr alloy established the highest strength with an ultimate tensile and yield tensile strength of 416 and 302 MPa, respectively.

References

[1] Lü, Y., Wang, Q., Ding, W., Zeng, X., Zhu, Y.: Mater. Lett., 44, 2000, p. 265.
doi:10.1016/S0167-577X(00)00041-0

[2] Friedrich, H., Schumann, S.: J. Mater. Process. Tech., 117, 2001, p. 276. doi:10.1016/S0924-0136(01)00780-4

[3] Mordike, B. L., Ebert, T.: Mater. Sci. Eng. A, 302, 2001, p. 37. doi:10.1016/S0921-5093(00)01351-4

[4] Bettles, C. J., Gibson, M. A.: Adv. Eng. Mater., 5, 2003, p. 859. doi:10.1002/adem.200310103

[5] Avedesian, M. M., Baker, H.: Magnesium and Magnesium Alloys. Materials Park, ASM International 1999.

[6] Maeng, D., Lee, J., Hong, S., Chun, B.: Mater. Sci. Eng. A, 311, 2001, p. 128.
doi:10.1016/S0921-5093(01)00921-2

[7] Gao, X., Nie, J.: Scripta Mater., 56, 2007, p. 645. doi:10.1016/j.scriptamat.2007.01.006

[8] Nayeb-Hashemi, A. A., Clark, J. B.: Binary Alloy Phase Diagrams. Mg-Y Phase Diagram. Materials Park, ASM International 1996.

[9] Okamoto, H., Prince, A., Villars, P.: Handbook of Ternary Alloy Phase Diagrams. Materials Park, ASM International 1997.

[10] Bae, D. H., Lee, M. H., Kim, K. T., Kim, W. T., Kim, D. H.: J. Alloys Compd., 342, 2002, p. 445. doi:10.1016/s0925-8388(02)00273-6

[11] Lee, J. Y., Lim, H. K., Kim, D. H., Kim, W. T., Kim, D. H.: Mater. Sci. Eng. A, 491, 2008, p. 349. doi:10.1016/j.msea.2008.02.010

[12] Xu, D. K., Tang, W. N., Liu, L., Xu, Y. B., Han, E. H.: J. Alloys Compd., 461, 2008, p. 248. doi:10.1016/j.jallcom.2007.07.096

[13] Kawamura, Y., Yoshimoto, S.: Magnesium Technology 2005. High Strength Mg-Zn-Y Alloys with LPSO Structure. San Francisco, TMS 2005.

[14] Kiguchi, T., Ninomiya, Y., Shimmi, K., Sato, K., Konno, T. J.: Mater. Trans., 54, 2013, p. 668. doi:10.2320/matertrans.MI201221

[15] Kim, J., Kawamura, Y.: Magnesium Technology 2010. Effects of Extrusion Conditions on the Microstructure and Mechanical Properties of Mg-Zn-Y-RE Alloys. New York, John Wiley & Sons 2010. doi:10.1002/9781118663004.ch35

[16] Leng, Z., Zhang, J., Sun, J., Shi, H., Liu, S., Zhang, L., Zhang, M., Wu, R.: Mater. Des., *56*, 2014, p. 495. doi:10.1016/j.matdes.2013.11.035

[17] Liu, H., Xue, F., Bai, J., Sun, Y.: Mater. Sci. Eng. A, *585*, 2013, p. 261. doi:10.1016/j.msea.2013.07.025

[18] Wang, J., Song, P., Gao, S., Wei, Y., Pan, F.: J. Mater. Sci., *47*, 2012, p. 2005. doi:10.1007/s10853-011-5998-2

[19] Lee, J. Y., Kim, D. H., Lim, H. K., Kim, D. H.: Mater. Lett., *59*, 2005, p. 3801. doi:10.1016/j.matlet.2005.06.052

[20] Itoi, T., Seimiya, T., Kawamura, Y., Hirohashi, M.: Scripta Mater., *51*, 2004, p. 107. doi:10.1016/j.scriptamat.2004.04.003

[21] Kawamura, Y., Kasahara, T., Izumi, S., Yamasaki, M.: Scripta Mater., *55*, 2006, p. 453. doi:10.1016/j.scriptamat.2006.05.011

[22] Gröbner, J., Schmid-Fetzer, R.: Metall. Mater. Trans. A, *44*, 2013, p. 2918. doi:10.1007/s11661-012-1483-z

[23] Zhang, Z., Liu, X., Hu, W., Li, J., Le, Q., Bao, L., Zhu, Z., Cui, J.: J. Alloys Compd., *624*, 2015, p. 116. doi:10.1016/j.jallcom.2014.10.177

[24] Sklenička, V., Kuchařová, K., Kvapilová, M., Svoboda, M.: Kovove Mater., *53*, 2015, p. 221. doi:10.4149/km-2015-4-221V